PROCEEDINGS OF THE SYMPOSIUM ON

THE CHEMISTRY AND PHYSICS OF ELECTROCATALYSIS

Edited by

J.D.E. McIntyre
AT&T Bell Laboratories
Murray Hill, New Jersey

M.J. Weaver
Department of Chemistry
Michigan State University
East Lansing, Michigan

E.B. Yeager
Department of Chemistry
Case Western Reserve University
Cleveland, Ohio

1984

PHYSICAL ELECTROCHEMISTRY DIVISION

Proceedings Volume 84-12

THE ELECTROCHEMICAL SOCIETY, INC., 10 South Main St., Pennington, NJ 08534-2896

THE ROLE OF OXYGEN AND OTHER CHEMISORBED SPECIES ON SURFACE PROCESSES FOR METALS AND SEMICONDUCTORS; APPROACHES TO DYNAMICAL STUDIES OF SURFACE PROCESSES.++

William A. Goddard III, John J. Low,* Barry Olafson, Antonio Redondo, Yehuda Zeiri,† Michael L. Steigerwald,‡ Emily A. Carter, Janet N. Allison,# and Roger Chang**

Arthur Amos Noyes Laboratory of Chemical Physics,§ California Institute of Technology, Pasadena, California 91125

Abstract: We examine some conceptual ideas useful in considering the chemistry of chemisorbed species (particularly oxygen) on surface processes. Topics analyzed include:(1) the surfaces of Si and GaAs and the oxidation of these surfaces, (2) surface oxides of metal surfaces and some possible processes in Ag-catalyzed epoxidation of ethylene, (3) the likely metal-oxide surface states of molybdates and of their possible roles in catalytic processes on these surfaces, (4) the role of transition metals in leading to facile allowed reactions, and (5) the oxidative addition of H_2 to a Pt complex as an illustration of how a metal can bring about the scission of the H-H bond with little or no activation barrier.

In addition, we outline the current state of progress in predicting dynamics of surface processes and the directions envisioned for simulating complex processes on realistic surfaces.

++ Presented at the 163rd Meeting of The Electrochemical Society, San Francisco, California, May 9, 1983.

* Exxon Fellow, 1983.

** National Science Foundation Predoctoral Fellow, 1982-1985; Shell Development Fellow, 1982-1983.

† Chaim Weizmann Postdoctoral Fellow, 1981-1983.

‡ Sun Oil Fellow, 1982-1983.

Fannie and John Hertz Foundation Predoctoral Fellow, 1979-1983.

§ Contribution No. 6863.

I. Introduction

A major objective in this paper will be to present some of the flavor of the multifarious modes of oxygen chemisorption on metals and semiconductors. In addition, we will examine the somewhat related chemisorption of NH_n and CH_n species on metals. The ultimate objective in studying chemisorption is to elucidate the mechanism and dynamics of reactive processes on surfaces, and we will outline some of the current ideas and new approaches to such studies.

II. Valence Bond Considerations

Wherever possible, we will reduce the results of detailed ab initio wavefunctions to simple valence bond concepts. This allows one to utilize these ideas not only to rationalize the systems being considered but also to make qualitative predictions about new processes.

In thinking about the bonding of oxygen states to surfaces, recall that the ground state of a free O atom is $(1s)^2(2s)^2(2p)^4$. We will find it useful to visualize the O atom in terms of the **valence bond diagram**

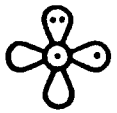

(1)

where the ∞ and O symbolize oxygen 2p orbitals in the plane and out of the plane, respectively, while the dots indicate the number of electrons. Configuration (1) is the ground state of oxygen atom since it allows the triplet ground state (Hund's rule), but occasionally (e.g., phosphine oxides) oxygen will bond as if it were in the singlet excited state with two doubly-occupied orbitals and an empty one, e.g.,

(2)

Also, in some circumstances the oxygen appears to oxidize the metal yielding a configuration corresponding to O^-,

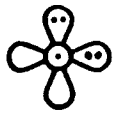

(3)

In bonding two oxygen atoms together, we combine configurations

such as (1), so that two singly-occupied p orbitals overlap to form a two-electron covalent bond as in

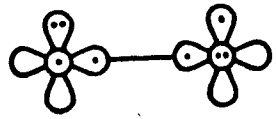

(4a)

or

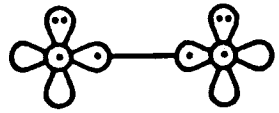

(5a)

Actually there is a second equivalent valence bond configuration corresponding to either (4a) or (5a)

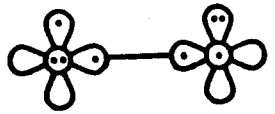

(4b)

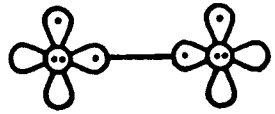

(5b)

so that the full wavefunctions involve the resonating configurations

(6)

and

(7)

This resonance effect is particularly large for (6) and results in (6) as the ground state of O_2 [1]. Because each configuration of (6) has two singly-occupied orbitals, it yields both a spin singlet and a spin triplet, and because the orbitals are orthogonal, the ground state is the triplet. The

bonding curves for the lower states of O_2 are shown in Figure 1; here $^3\Sigma_g^-$ and $^1\Delta_g^-$ arise from (6) [as do $^3\Delta_u^-$ and $^1\Sigma_u^-$], while $^1\Delta_g^+$ and $^1\Sigma_g^+$ arise from (7) [as do $^3\Delta_u^+$ and $^3\Sigma_u^+$].

Despite the fact that O_2 is a triplet state, one should not think of it as a diradical. Rather, these unpaired electrons are intimately involved in the bonding. Indeed, of the total 119 kcal involved in the O=O bond, about 47 kcal can be considered as the sigma bond, while 72 kcal involves the π electrons (mostly resonance). The first step of reacting the O_2 with something generally requires losing most or all of the π resonance energy, causing the O_2 to be far less reactive than would normally be expected for a triplet (biradical) molecule. Indeed, it is this process of decreasing the O_2 π resonance that generally forms the critical step in activating the O_2 bond.

For example, in bonding a radical R, such as H or CH_3 to O_2, we would bring the radical up to overlap one of the singly-occupied O_2 orbitals, as in

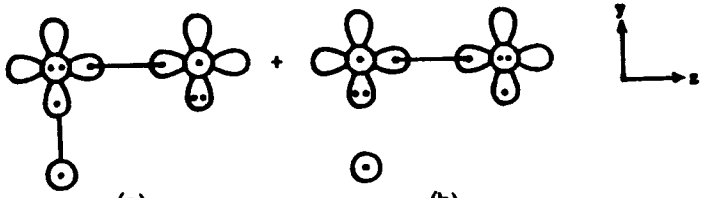

(a) (b) (8)

However, of the two resonance configurations, only the left one is bonding. Thus bonding to R causes most of the O_2 π resonance to be lost, leading to the VB configuration

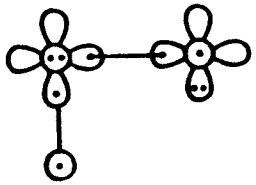

(9)

The result is an R-O_2 bond, which is weakened by about 54 kcal due to this loss in O_2 π resonance, e.g. [2,3],

$$D(H\text{-}O_2) = 50 \text{ kcal} = 104 - 54$$

$$D(Me\text{-}O_2) = 29 \text{ kcal} = 83 - 54.$$

It is this loss of resonance that is responsible for the large activation barrier to activating O_2. Thus, the first step of O_2 abstracting an H or Me from

some gas phase species X-H or X-CH_3 would be thermoneutral only for extremely weak X-H or X-CH_3 bonds (50 or 29 kcal). Surfaces, however, have other options, as we will see.

One way to view the activation of O_2 is in terms of the reduced O-O bond energy, e.g., [3,4]

$$D(HO\text{-}O) = 66 \text{ kcal}$$

$$D(HO\text{-}O^-) \approx 83 \text{ kcal}$$

$$D(O\text{-}O^-) = 95 \text{ kcal}$$

which can be compared with

$$D(O\text{-}O) = 119 \text{ kcal}$$

and

$$D(HO\text{-}OH) = 51 \text{ kcal}.$$

Clearly, atom transfer is more effective than electron transfer in weakening the OO bond.

III. Semiconductor Surfaces

First we will examine the interaction of O and O_2 with semiconductor surfaces. This is a good place to start since geometric considerations of the surface very nearly specify the electronic structure.

A. Silicon

Despite 23 years of careful experiment and of theoretical rationalization, there are still *considerable* uncertainties about the detailed structure of even the simple (111) and (100) surfaces of Si [5-10]. However, most current models lead to the idea that after reconstruction, each surface Si atom has three of its four possible neighbors, leading to one electron in a dangling bond orbital,

(10)

Thus the first step of bonding to O_2 is much as in (8) and (9), leading to a peroxy radical initial state for the perfect surface [11].

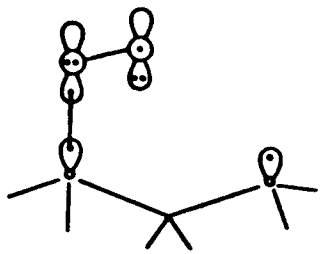

(11)

Even for the perfect surface, various subsequent steps of oxidation are quite exothermic, as indicated in Figure 2.

The calculations indicate that the surface peroxy radical species (11) would have a barrier to closing to form a bridged peroxide species, that in turn could cleave to form surface oxides, which could then insert in Si-Si bonds to initiate oxidation. However, the excited state (0.9 eV higher) in (12)

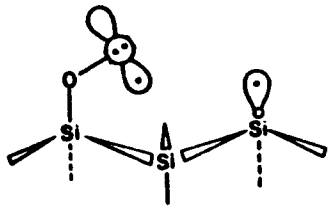

(12)

Peroxy radical

Excited state

need not have a barrier. On the other hand, calculations suggest [12] that the reduced species (13a)

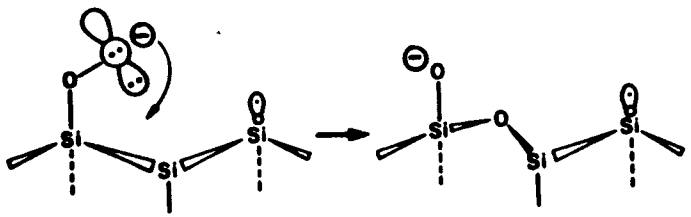

(13)

(a) Superoxide **(b)**

leads to a more facile insertion in Si-Si bonds than (11).

B. GaAs

Although bulk GaAs has the same tetrahedral structure as Si, its surfaces are quite different. Thus the cleavage surface is (110) [rather than (111)] with each surface Ga bonded to three As and each surface As bonded to three Ga. However, rather than singly-occupied dangling bond orbitals at the surface, the As and Ga adopt neutral electronic configurations where each surface As has a 4s lone pair (plus three covalent As-Ga bonds), and each surface Ga has an empty orbital (plus the covalent Ga-As bonds). The net result is that the surface reconstructs so that the surface As moves away from the surface (adopting a pyramidal 95° average bond angle) and the surface Ga moves into the surface (adopting a nearly planar configuration) [13-15]. The resulting surface has the character illustrated in (14) where the reconstruction energy is 1.36 eV per surface As. The surface As has a lone pair pointing out from the surface and should act as a Lewis base (a nucleophile) so that acid attack might prefer this site. On the other hand, the surface Ga has an empty orbital and should act as a Lewis acid (an electrophile) so that base attack might prefer this site.

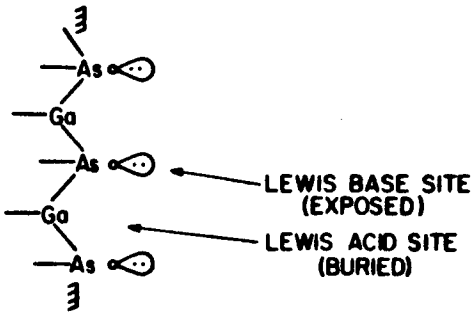

(14)

Reactions at this surface may lead to formation of tetrahedral As and Ga, but in so doing the reaction must overcome the 1.36 eV reconstruction energy (requiring strong chemisorption).

As a photoelectrode, the active GaAs surface site may be visualized as in (15)

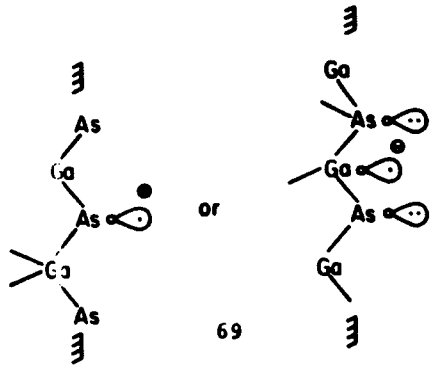

(15)

for the anode or cathode, respectively (in both cases the surface configuration distorts toward the unreconstructed tetrahedral geometry).

The perfect surface in (14) has no dangling bond orbital needed for the first one-electron step in activating O_2. Indeed, experimental evidence indicates that chemisorption of O_2 on GaAs is dominated by defect sites (presumably with dangling bond radical sites) [16]. As with Si, GaAs is readily oxidized, but, just as with Si, one can (under UHV conditions) form a stable surface oxide with about one monolayer of oxygen [17,18]. Speculation is that this surface oxide involves an arsine-oxide type donor-acceptor bond [19] (16a)

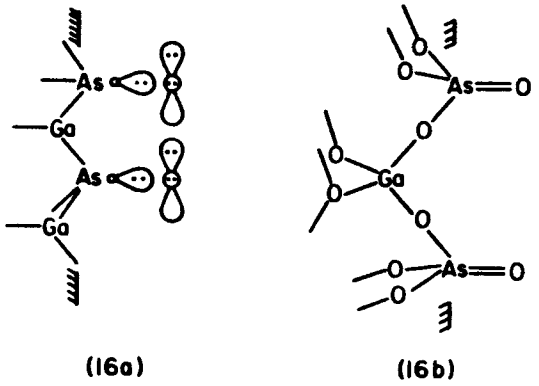

(16a) (16b) (16)

to the surface As atoms. Although some experimental evidence supports this idea [20], no mechanism has been presented for how the surface species (16a) is formed from O_2. Calculations [21] on Cl_3PO, Cl_3AsO, and Cl_3SbO indicate M=O bond energies of 114, 82, and 63 kcal/mole, suggesting that surface species of the form (16a) are highly favorable on phosphides (e.g., GaP), tenable for arsenides (e.g., GaAs), but unlikely for antimonides (e.g., InSb). The final state of oxidizing the GaAs at low temperature might be as in (16b) [At high temperature, preferential evaporation of As_2O_3 leads to a Ga-rich surface]

IV. Metal Surfaces

A. Chemisorbed NH_n and CH_n

Before examining states of chemisorbed O, we will consider states of chemisorbed NH_n and CH_n. Particularly interesting is the tendency to form strong metal-adsorbate π bonds, (17).

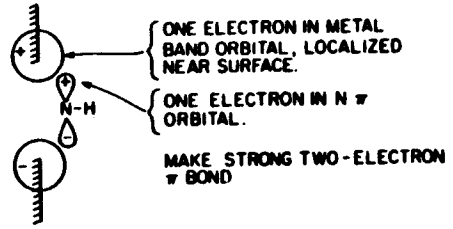

(17)

Thus free NH has the valence bond diagram

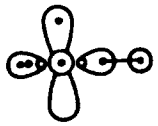

(18)

and on the surface it stands upright so as to form two strong π bonds to the metal (see Figure 3) [22]. Meanwhile, the 2s lone pair is nearly unchanged upon bonding to the surface.

Next consider chemisorbed CH. The valence bond configuration of CH suitable for forming maximal bonding is

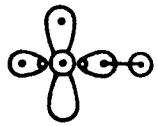

(19)

with singly-occupied σ, π_x, and π_y orbitals. As expected from (18), the surface makes two strong π bonds to CH (see Figure 4) [22]. However, the sigma bond to adsorbed C is very similar to that for adsorbed NH. Thus, in a sense it is as if CH abstracts an electron to obtain the electronic configuration of CH^-,

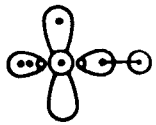

(20)

which then bonds to the surface. On the other hand, since the C is only 0.7 Å from the surface [22], this extra electron is still effectively at the metal surface so that the metal has not really been ionized. Rather, the surface electrons are rearranged to localize near the carbon.

Similarly, the bond of H to the surface yields a pair of electrons localized near the H but with very little net charge transfer (see Figure 5).

For N and C the bonding is similar to that of NH and CH, with two strong π bonds and a surface-σ pair [22]. In both cases the electronic structure resembles that of the anion N^- or C^-. For example, the orbitals of Ni_3N are shown in Figure 6 [22].

Some general features of these studies [22-24] are that:

1) electrophilic species such as Cl, S, O, N, H, and C prefer high coordination sites with three or four nearest neighbor metal atoms,

(21)

while

2) nucleophilic species such as CO tend to prefer low coordination sites (often on-top sites).

(22)

B. Chemisorbed O

Just as with N and C, so we find that chemisorbed O effectively localizes the additional electron from the surface to obtain the character [24] of O^-. However, an interesting aspect of the O system is the presence of *two* low lying states [24].

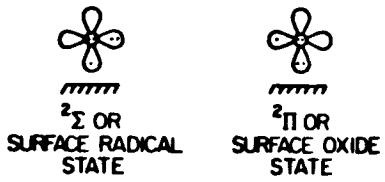

(23)

Each state has five electrons distributed over the three p orbitals, leading to a singly-occupied p orbital either perpendicular to the surface ($^2\Sigma^+$ state) or parallel to the surface ($^2\Pi$ state) [25]. In the latter case, a π

bond can be formed with the surface, leading to a strong, short bond. However, it appears that in some situations both chemisorbed states of oxygen may be stable [24]. The $^2\Sigma^+$ state leads to a radical (singly-occupied) orbital perpendicular to the surface and should be extremely reactive. Consequently, this state is referred to as the **surface radical state**. The $^2\Pi$ state leads to a π bond with the surface and hence should be more stable and less reactive. This state is referred to as the **surface oxide state**. This latter state may have only a small barrier to penetrating the surface where it is generally most stable in a site between the top two metal layers (the **subsurface oxide state**). In this state the polarity of the metal-oxygen bonds makes the surface atoms more positive, leading to enhanced bonding of Lewis bases to the surface.

The general sequence for reactions of O_2 with a metal surface is illustrated in Figure 7.

C. Epoxidation of Ethylene over Ag

As an illustration of how these different states of oxygen may play a role in surface chemistry, consider the epoxidation of ethylene over supported Ag catalysts [26,27]:

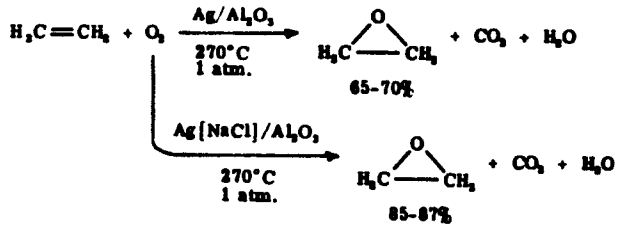

(24)

Although this process can be made 90% selective under appropriate conditions, there is currently little understanding of the detailed mechanism.

Based on calculations of various O and O_2 species on Ag and based on simple considerations of various mechanistic steps [28], we believe that the three oxygen species illustrated in (25) may play a role.

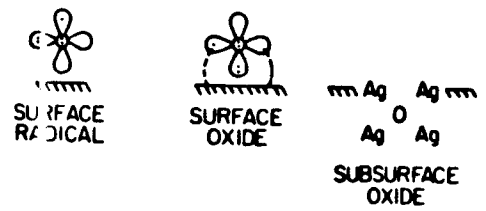

(25)

The surface radical should be an ideal species for the radical sequence of (26).

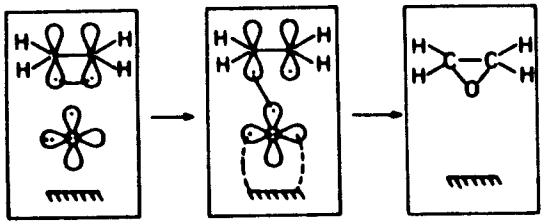

(26)

leading to direct formation of epoxide, whereas both the surface oxide and subsurface oxide may prefer an H-abstraction step that would lead to complete combustion, (27),

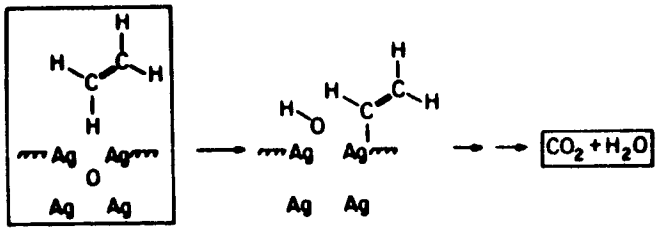

(27)

If the surface radical species is important, then it is important to consider how it is stabilized. Crude calculations [28] suggest that it is unstable with respect to the surface oxide state; however, presence of subsurface oxide or of surface oxide might stabilize this state, as illustrated in (28). In particular, the Cl promoter effect in (24) may be due to stabilization of this state, as indicated in (28).

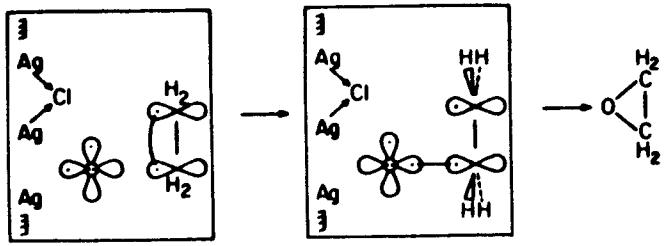

(28)

Although these discussions are highly tentative, they should illustrate how to use ideas about chemisorbed species to reason chemically about surface reactions.

V. Molybdates

Molybdates are used for a number of catalytic processes and, in particular, bismuth molybdates (e.g., $Bi_2Mo_3O_9$) have been used for selective oxidation [29],

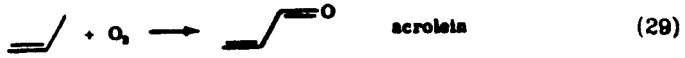

(29)

and ammoxidation [30]

(30)

In order to understand the surface chemistry of such species, it is important to note that there are two quite distinct types of molybdenum oxygen species at the surface [31],

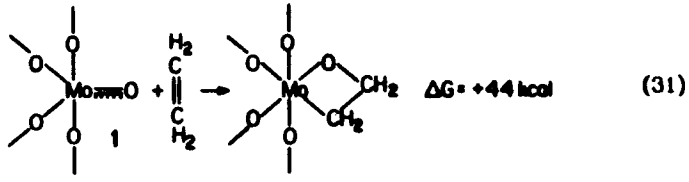

(31)

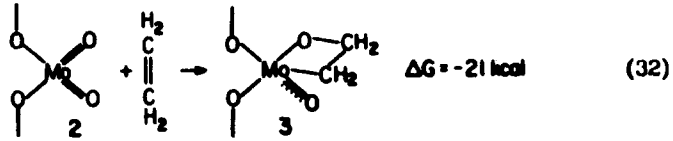

(32)

One type **(1)** has four single bonds (partially ionic) to bridging oxygens and one short covalent metal oxygen multiple bond, while the other **(2)** has two single bonds to bridging oxygens and two short covalent metal oxygen multiple bonds. Despite the fact that both types have the Mo fully oxidized (Mo^{6+}), the chemistries at these two sites are dramatically different, as indicated in Eqs. (31) and (32). The reason for this enormous chemical difference is that the Mo=O bonds in **1** and **2** are dramatically different. The two Mo=O bonds of **2** are both covalent double bonds consisting of a σ and a π bond, just as in $H_2C{=}O$. However, the Mo=O bond in **1** is a partial triple bond consisting of two π bonds plus a donor-acceptor sigma bond. The result is a bond about 30 kcal stronger [31,32]. The origin of this difference can be understood by noting that both Mo sites make a *total* of two π bonds. The difference is that **2** must *share* these π

bonds between two oxo groups, leading to one π bond each, while **1** may use both π bonds for the same oxo group, forming a partial triple bond.

However, these differences in bonding for **1** and **2** account only for about half of the energetic differences between (31) and (32). The other half involves the ***spectator oxo effect*** [31], which can be understood by examining **3**. There are four single bonds to the Mo plus the bond to the spectator oxo group (the one that did *not* react). Since only the spectator oxo group in **3** makes both π bonds, this spectator oxo group can make two π bonds plus the σ can bond, leading to a partial triple bond. However, in the reactant **2**, each of the two oxo groups competes for the two π bonds so that each Mo=O bond is a double bond. Thus **the spectator oxo group changes from a double to a triple bond** during the reactions and thereby **stabilizes the intermediate 3** by ~ 30 kcal (our most complete calculations suggest a stabilization of 35 kcal) [32].

Recent studies [32] show similar, albeit smaller (15 kcal), spectator stabilization effects for Mo=NH bonds, indicating that species such as

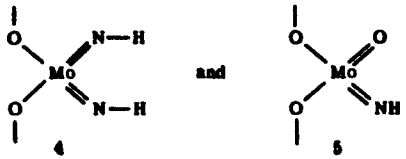

(33)

are much more reactive than **1** or

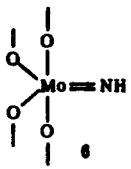

(34)

There are indications that such species as **2**, **4**, and **5** may be involved in reaction 30 [30,32].

VI. Reaction Mechanisms

Although there is not yet a good detailed understanding of the nature of reactions on surfaces, there has been some recent progress in understanding the details of concerted reactions on transition metal clusters that may be relevant to related reactions on surfaces.

The first question concerns whether there **are** selection rules for reactions at transition metal centers. Thus it is well known [33,34] that reactions such as

(35)

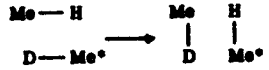

(36)

are forbidden, whereas there are several examples where analogous reactions seem to be quite facile when a transition metal is involved. Recent studies [35] of a number of reactions such as

$$Cl_2Ti^+-H + D-D \rightarrow Cl_2Ti^+-D + H-D \qquad (37)$$

$$ClMn-H + D-D \rightarrow ClMn-D + H-D \qquad (38)$$

show that such reactions are allowed **if** the metal-hydrogen bond is covalent ***and*** dominantly d in character. The reason for this is illustrated in Figure 8 where we see that during the reaction both bond pairs delocalize and relocalize without ever destroying the large overlap in the bond. To do this requires a d orbital, as is clear in Figure 8b. These results suggest that 2 + 2 suprafacial reactions such as in the Cossee mechanism of Ziegler-Natta polymerization [36]

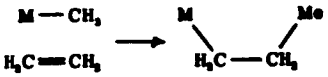

(39)

and steps such as

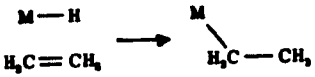

(40)

(41)

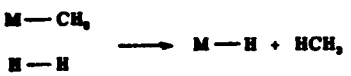

(42)

will be concerted if the ligands to M are such as to stabilize a covalent d-like bond on the M. The strategy in designing a specific catalytic process is then to choose metals and ligands that build in this character at the appropriate time to do the desired chemistry.

In order to obtain some insight into the oxidative addition to and the reductive elimination from metals, we examined (43) [37]

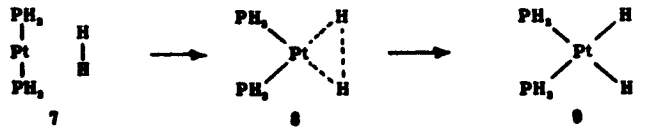

(43)

The potential surface for motion along the reaction path is shown in Figure 9. The overall process of **7** to **9** is exothermic by 16.2 kcal, comparable to the value ΔH = -22 kcal obtained for Ni surfaces. For the process (43) we calculate a small activation barrier of 4.0 kcal (for correlated wavefunctions, this activation barrier gets smaller).

It is interesting that up to the saddle point the H_2 bond length is unchanged, remaining at 0.74 ± 0.01 A. In this process the phosphines bend back out of the way of the H_2 (from 180° to 137°), providing a Lewis acid site (Pt d^{10}) to bond to the H_2 (a Lewis base here). From the saddle point (C) to point B the phosphines bend further back (to 111°) and in so doing stabilize the s^1d^9 state of Pt (rather than d^{10}) which can make two covalent Pt-H bonds, allowing the H_2 bond to break (H-H increases to 1.09 A). From B to A the energy drops rapidly as the Pt-H bonds decrease to the equilibrium positions (1.50 A).

These results suggest that the reaction path for dissociative chemisorption of H_2 on a metal surface might be as in Figure 10.

VII. Graphically Assisted Reactions and Dynamics Simulation (GARDS)

The previous discussion has emphasized the atomic-level mechanistic considerations upon which we have focused in recent years. This work has, we believe, provided some useful insights into important steps in surface processes, and such work will continue to be valuable. However, the difficult challenges in developing new materials and catalysts involve balancing and optimizing a number of chemical processes that occur simultaneously with each other and which may enhance or annihilate other processes. Consequently we believe that the major theoretical challenge in the next decade will be to develop a reliable procedure for simulating the multifarious competing chemical processes occurring on real surfaces. There are five basic elements of this approach.

1. Surface Model - One must include at least 10,000 surface (and subsurface) atoms in order to properly describe the variety of steps, kinks, impurity sites, and variations in composition that may occur on a real surface. Such large clusters preclude the use of quantum chemistry calculations to obtain the energy surfaces.

2. Force Field - One must account for the atom-atom interactions in terms of long-range two-body forces plus short-range three-body and four-body valence terms in a form that allows the calculation of forces on all 10,000 atoms in a few seconds.

3. Classical Dynamics - Given the forces and initial conditions, one can predict the trajectories of all primary atoms using classical equations of motion.

4. Stochastic Limits - In order to consider the long time scale for many-surface processes, one needs to replace secondary surface atoms (that do not play a direct role in dynamics but serve as heat sink or source) to obtain Langevin equations involving only the primary atoms (the secondary atoms lead to friction and random force terms).

5. Graphics display - In order to extract chemical understanding of the processes in this simulated system, we must be able to view the full 10,000-30,000 atom system on a vector graphics display that can zoom in on an active site and rotate and translate the view to follow the chemistry as the atomic coordinates evolve in time.

A typical mode for carrying out studies using such simulations will be as follows:

1) The computer uses the general *force field* to evaluate the forces on all atoms at a given instant, takes the appropriate *stochastic limits* for non-essential degrees of freedom (describing, for example, the bulk atoms comprising the energy sink or source), and calculates the locations of the various atoms at the next time step (with the current values for velocities) using *classical (generalized Langevin) equations of motion*.

2) At appropriate time steps, a corrected set of coordinates (time averaged to eliminate simple vibrations) is passed from the computer to the vector graphics system. The screen of the graphics system is continually refreshed with the current coordinates so that the user "sees" the reaction as it proceeds and interactively examines the reactive system to follow the dynamics of the reaction.

3) The graphics terminal is a vector system that can display the whole reactive system, zoom in on a selected portion of this system, and rotate and translate the view to find the critical regions. This graphics system automatically cuts away extraneous atoms of the reactive system and automatically lets more distant atoms fade away in intensity. It color codes the atoms so that one can recognize instantly the composition and identity of the various species.

4) From the perspective of the user, he is watching the reaction as it proceeds. He can then interactively modify preselected variables to request the computer to modify surface temperature, gas temperature, pressure, vapor composition, or intensity of external laser or ion beams. By following the subsequent dynamics he can determine the impact of these changes upon various reactions.

This overall procedure is referred to as ***Graphically Assisted Reactions and Dynamics Simulation (GARDS)***. Current progress in developing GARDS is as follows:

1) We are developing automatic programs for representing surfaces for various crystal structures by simply specifying the Miller indices and structure type [38]. Geometries at interfaces and at surface defects will be obtained by energy minimization using the force field.

2) We currently have crude force fields for H, C, N, and O plus such metals as Zn, Ca, Fe, etc. We have used these to describe the structures for some enzyme-substrate systems as discussed below [39]. We are developing a new scheme for force fields where the long-range two-body terms are obtained directly from accurate theoretical calculations (this includes van der Waals attraction and Pauli repulsion). The short-range valence forces are then obtained from calculations on small clusters by subtracting the two-body interactions and fitting the residue [40].

3) The classical dynamics programs use conjugate gradient techniques to rapidly search out optimum structures. For an enzyme with 2500 non-hydrogen atoms, these programs can currently calculate time steps in 30 seconds on a VAX 11/780.

4) We have been able to describe the dynamics of desorptive processes at the gas/solid interface by taking appropriate stochastic limits *(vide infra)* [41,42] and are currently formulating this theory for the liquid/solid interface [43].

5) We are currently developing the software for flexible graphics display of the molecules as the dynamics proceed [44].

In order to indicate the current state of affairs, we will describe two recent results.

A. Thermolysin

Thermolysin is a protease that cleaves peptide bonds

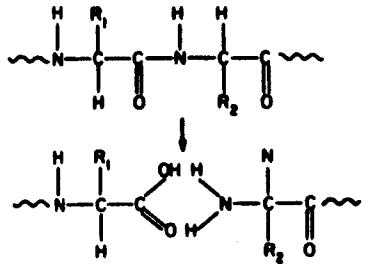

(44)

(selective for cases with medium-sized nonpolar side chains, such as valine, leucine, and isoleucine with R_2 = iPr, iBu, and sBu, respectively). It has 2437 non-hydrogen atoms including a Zn at the active site and four Ca's. Several crystal structures with and without inhibitor have been reported [45]. Figures 11 and 12 show the close agreement between the theoretical [39] and x-ray structures [45], while Figure 13 shows the calculated structure with an inhibitor bound to the active site [39]. Given the theoretical force field, we can examine how the active site is modified when the enzyme is attached to supports in various ways, knowledge that would be useful in developing ways to immobilize such enzymes for biocatalysis applications.

B. Classical Stochastic Diffusion Theory Approach to Surface Dynamics

A major problem in using classical dynamics to simulate chemical processes is that the time scale in doing the dynamics must be short compared with vibrational periods (10^{-12} sec), whereas some important processes might require time scales as long as 1 sec. Consequently, it is essential to develop approaches that allow the vibrational modes to be properly averaged in doing the dynamics while still allowing these modes to serve as heat reservoirs. In order to illustrate our current approach, consider the desorption of a particle, e.g., CO, from a surface.

The classical equation of motion for the CO can be written as

$$\mu\ddot{R} = -\frac{\partial V}{\partial R}(R, \zeta, z) \ , \tag{45}$$

where R, ζ, and z symbolize the coordinates of the CO, the primary (adjacent) solvent molecules, and the primary (adjacent) surface atoms,

respectively. Identifying the adjacent surface atoms as primary and all other surface atoms as secondary, we can write the equation of motion for the primary surface atoms [41,42,46] as

$$M_s\ddot{Z} = -M_s\Omega_s^2 Z - \frac{\partial V(R,\zeta,Z)}{\partial Z} - M_s\beta_s\dot{Z} - F_s(t) \ , \qquad (46)$$

where the last two terms include the friction and random force terms due to the secondary surface atoms. Similarly, identifying the adjacent solvent molecules as primary and the more distant solvent molecules as secondary, we can write the equation of motion of the primary solvent molecules as [43]

$$M_i\ddot{\zeta}_M = -M_i\Omega_i^2\zeta_M - \frac{\partial V}{\partial\zeta_M}(R,\zeta,z) - M_i\beta_i\dot{\zeta}_M + F_i(t) \ , \qquad (47)$$

where the last two terms are the friction and random forces due to secondary solvent molecules. Solving Eqs. (46) and (47) formally (assuming harmonic interactions in the solid and liquid, using Laplace transforms, and taking the Markovian limit) and substituting into (43) leads to an effective equation of motion of the form [41-43]

$$\ddot{R} = -\omega^2 R - \left[\frac{6kT}{\mu D_i} + \frac{M_s\beta_s}{\mu}\right]\dot{R} + f(t) \ , \qquad (48)$$

where ω^2 is an effective vibrational frequency (modified by the average over solid and liquid vibrational modes) and the factor multiplying $\dot{R}$ involves the friction due to the liquid and the solid. Solving the generalized Liouville equation for the probability distribution over positions and velocities of the adparticle in the steady-state limit (using the boundary condition that desorbed particles do not readsorb) leads to a net rate equation of the form [43,47,48]

$$\text{rate desorption} = \left[\frac{\Omega_0}{2\pi}\right]\left[\frac{2\mu l^2\Omega_r^2}{kT}\right]\left[e^{-D_e/kT}\right]T(T) \ , \qquad (49)$$

where

a) $\frac{\Omega_0}{2\pi}$ is the surface adsorbate vibrational frequency as modified by adsorbate-solid adsorbate-solvent interactions,

b) $[2\mu l^2\Omega_r^2/kT]$ involves the frustrated rotation (or bending) mode of the adsorbed molecule at the surface [47],

c) D_e is the desorption enthalpy, and

d) T(T) involves the friction properties of the solid and solvent. For the gas-surface interface [41,42] $T(T) \approx 1$, whereas for the liquid/surface interface, T(T) depends sensitively on the mass and vibrational frequency of the adsorbate (μ and Ω_0) and on the viscosity of the solvent [43].

As an illustration, we compare in Figure 14a the predicted and experimental desorption rates of CO from the Ni(110) gas/surface interface [41,42]. The agreement is excellent; moreover, the theory explains the anomalously high frequency factor of $\sim 10^{16}\ sec^{-1}$ observed in the experiments. Energy in the frustrated rotation mode (see [41]) can convert to translational energy for desorption leading to an extra factor of 100 in the preexponential factor, as indicated in Figure 14b. [Thus, the desorbing molecule has only half the rotational energy normal for temperature T.] With this theory we can calculate directly the temperature programmed desorption spectra that would be observed in experimental studies of desorption rates. An illustration [48] of this is given for NH_3/Ni(111) in Figure 15. We are in the process of developing the equations for reactions at liquid/surface interfaces [43] and are including the effect of applied potentials upon the rates. This would allow us to calculate directly such experimental observables as the cyclic voltammogram.

VIII. Summary

Some of the points we would like to emhasize here are

1) **Oxygen is not a round blob.** In order to understand the variety of different roles that oxygen plays on surfaces, it is essential to think of oxygen in terms of its constituent atomic orbitals and to consider where the electrons are, as summarized in Figure 16. We should not picture O atom as a round blob of electron density stuck here or there upon the surface.

2) **Theory is starting to play a useful role** in elucidating surface processes. On the one hand, theory can now provide reliable quantitative answers for some questions that are most difficult to answer experimentally (e.g., geometry and energy of a reaction intermediate). Equally important, however, the theory is leading to a conceptual framework encompassing both theoretical and experimental data that can be used to predict and design systems in advance of experiment.

3) Theoretical simulations of real surface processes seems feasible. There are numerous difficulties to overcome before practical simulations will be possible; however, each of these problems seems solvable.

IX. Acknowledgments

This paper has brought together the results of a number of studies funded by several agencies:

a) Semiconductor surfaces and oxidations: Office of Naval Research (Contract No. N00014-79-C-0797);

b) Chemisorption and oxidation of metal surfaces and oxidative addition of H_2 to Pt: National Science Foundation (Grant Nos. DMR79-19689 and DMR82-15650);

c) Epoxidation over Ag: Shell Development Corporation;

d) Molybdate surfaces: Petroleum Research Fund of the American Chemical Society (Grant No. 13110-AC5,6);

e) Spectator oxo effect and concerted reactions: National Science Foundation (Grant No. CHE80-17774);

f) Dynamics of gas-surface reactions: Department of Energy (Contract No. DE-AM03-76SF00767; Project Agreement No. DE-AT03-80ER10608); and

g) Graphically assisted reactions and dynamics simulation: Department of Energy, Energy Conservation and Utilization Project, Jet Propulsion Laboratory.

It is also important to acknowledge the earlier work by Dr. Thomas H. Upton (now at Exxon), Professor Anthony K. Rappe' (now at Colorado State University), Dr. Coenraad Swarts (now at Shell Development), and Professor Thomas C. McGill (Caltech) in various areas touched upon herein.

References

1. B. J. Moss and W. A. Goddard III, *J. Chem. Phys.*, **63**, 3523 (1975).

2. W. A. Goddard III and L. B. Harding, in *Biochemical and Clinical Aspects of Oxygen*, W. A. Caughey, Ed. (Academic Press, Inc., New York, 1979), pp. 513-555; W. A. Goddard III and B. D. Olafson, *Ann. N. Y. Acad. Sci.*, **367**, 419 (1981).

3. As reference bond energies, we use D(H-OMe) = 104 kcal and D(Me-OMe) = 83 kcal, so that 1-3 nonbonded interactions are properly included.

4. D. F. McMillan and D. M. Golden, *Ann. Rev. Phys. Chem.*, **33**, 493 (1982); M. W. Chase *et al.*, *J. Phys. Chem. Ref. Data*, **11**, 695 (1982).

5. K. C. Pandey, *Phys. Rev. Lett.*, **47**, 1913 (1981); *ibid.*, **49**, 224 (1982).

6. G. Binning, H. Rohrer, Ch. Gerber, and E. Weibel, *Phys. Rev. Lett.*, **50**, 120 (1983).

7. R. Feder, *Solid State Commun.*, **45**, 51 (1983).

8. W. S. Yang, F. Jona, and P. M. Marcus, *Solid State Commun.*, **43**, 847 (1982).

9. A. Redondo, W. A. Goddard III, and T. C. McGill, *J. Vac. Sci. Technol.*, **21**, 649 (1982); *Surf. Sci.*, in press.

10. A. Redondo and W. A. Goddard III, *J. Vac. Sci. Technol.*, **21**, 344 (1982).

11. W. A. Goddard III, A. Redondo, and T. C. McGill, *Solid State Commun.*, **18**, 981 (1976).

12. A. Redondo, W. A. Goddard III, C. A. Swarts, and T. C. McGill, *J. Vac. Sci. Technol.*, **19**, 498 (1981).

13. A. R. Lubinsky, C. B. Duke, B. W. Lee, and P. Mark, *Phys. Rev. Lett.*, **36**, 1058 (1976); S. Y. Tong, A. R. Lubinsky, B. J. Mrstik, and M. A. Van Hove, *Phys. Rev. B*, **17**, 3303 (1978); A. Kahn, E. So, P. Mark, C. B. Duke, and R. J. Meyer, *J. Vac. Sci. Technol.*, **15**, 1223 (1978); D. J. Miller and D. Haneman, *ibid.*, **15**, 1267 (1978); R. J. Meyer, C. B. Duke, A. Paton, A. Kahn, E. So, J. L. Yeh, and P. Mark, *Phys. Rev. B*, **19**, 5194 (1979).

14. C. A. Swarts, W. A. Goddard III, and T. C. McGill, *J. Vac. Sci. Technol.*, **19**, 360 (1981).

15. C. A. Swarts, T. C. McGill, and W. A. Goddard III, *Surf. Sci.*, **110**, 400 (1981).

16. W. A. Goddard III, J. J. Barton, A. Redondo, and T. C. McGill, *J. Vac. Sci. Technol.*, **15**, 1274 (1978).

17. See, for example, F. Meyer and M. J. Sparnaay, in *Surface Physics of Phosphors and Semiconductors*, edited by C. G. Scott and C. E. Reed (Academic, New York, 1975), p. 321; H. Ibach, K. Horn, R. Dorn, and H. Luth, *Surf. Sci.*, **38**, 433 (1973); F. J. Himpsel, P. Heimann, T.-C. Chiang, and D. E. Eastman, *Phys. Rev. Lett.*, **45**, 1112 (1980); C.-Y. Su, P. R. Skeath, I. Lindau, and W. E. Spicer, *J. Vac. Sci. Technol.*, **18**, 843 (1981) and private communication.

18. P. Pianetta, I. Lindau, C. Garner, and W. E. Spicer, *Phys. Rev. Lett.*, **35**, 1356 (1975); W. E. Spicer, P. Pianetta, II Lindau, and P. W. Chye, *J. Vac. Sci. Technol.*, **14**, 885 (1977); P. W. Chye, P. Pianetta, I. Lindau, and W. E. Spicer, *ibid.*, **14**, 917 (1977).

19. J. J. Barton, W. A. Goddard III, and T. C. McGill, *J. Vac. Sci. Technol.*, **16**, 1178 (1979).

20. J. Stohr, R. S. Bauer, J. C. McMenamin, L. I. Johnansson, and S. Brennan, *J. Vac. Sci. Technol.*, **16**, 1195 (1979).

21. R. Chang and W. A. Goddard III, to be published.

22. J. J. Low and W. A. Goddard III, to be published.

23. T. H. Upton, W. A. Goddard III, and C. F. Melius, *J. Vac. Sci. Technol.*, **16**, 531 (1979); T. H. Upton and W. A. Goddard III, *CRC Critical Reviews in Solid State and Materials Science*, **10**, 261 (1981).

24. T. H. Upton and W. A. Goddard III, *Phys. Rev. Lett.*, **46**, 1635 (1981).

25. This is analogous to the states of alkali oxide diatomics M^+O^- where the corresponding $^2\Pi$ and $^2\Sigma^+$ states are nearly degenerate. See J. N. Allison and W. A. Goddard III, *J. Chem. Phys.*, **77**, 4259 (1982).

26. A. M. Brownstein, *Trends in Petroleum Technology* (Petroleum Publishing Company, Tulsa, Oklahoma, 1976).

27. A. Ayame, N. Takeno, and H. Kanoh, *J. Chem. Soc., Chem. Commun.*, 617 (1982).

28. E. A. Carter and W. A. Goddard III, to be published.

29. R. K. Grasselli and J. D. Burrington, *Advan. Catal.*, **30**, 133 (1981).

30. J. D. Burrington, C. T. Kantisek, and R. K. Grasselli, *J. Catal.*, **63**, 235 (1980).

31. A. K. Rappe' and W. A. Goddard III, *J. Am. Chem. Soc.*, **104**, 448 (1982).

32. J. N. Allison and W. A. Goddard III, to be published.

33. R. B. Woodward and R. Hoffmann, *The Conservation of Orbital Symmetry*, (Academic Press, New York, 1970).

34. W. A. Goddard III, *J. Am. Chem. Soc.*, **94**, 793 (1972).

35. M. L. Steigerwald and W. A. Goddard III, *J. Am. Chem. Soc.*, submitted for publication.

36. J. Soto, M. L. Steigerwald, and R. H. Grubbs, *J. Am. Chem. Soc.*, **104**, 4479 (1982).

37. J. J. Low and W. A. Goddard III, to be published.

38. E. T. Knight and W. A. Goddard III, to be published.

39. B. D. Olafson, W. A. Goddard III, and J.Snyder, to be published.

40. M. J. Brusich and W. A. Goddard III, to be published.

41. A. Redondo, Y. Zeiri, and W. A. Goddard III, *Phys. Rev. Lett.*, **49**, 1847 (1982).

42. Y. Zeiri, A. Redondo, and W. A. Goddard III, *Surf. Sci.*, in press; A. Redondo, Y. Zeiri, and W. A. Goddard III, *ibid.*, submitted for publication.

43. Y. Zeiri, A. Redondo, and W. A. Goddard III, *J. Electrochem. Soc.*, to be submitted.

44. B. D. Olafson and W. A. Goddard III, to be published.

45. B. W. Mathews, L. H. Weaver, and W. R. Kester, *J. Biol. Chem.*, **249**, 8030 (1974).

46. S. A. Adelman and J. D. Doll, *J. Chem. Phys.*, **61**, 4242 (1974); *ibid.*, **63**, 4908 (1975); *ibid.*, **64**, 2375 (1976); *Accts. Chem. Res.*, **10**, 378 (1977); J. C. Tully, *Ann. Rev. Phys. Chem.*, **31**, 319 (1980); B. J. Garrison and S. A. Adelman, *J. Chem. Phys.*, **67**, 2379 (1977).

47. This differs by a factor of $\pi/4 = 0.8$ from the form reported in Refs. 41 and 42 due to a different way of averaging over the limits of the harmonic frustrated-rotation mode.

48. A. Redondo, Y. Zeiri, J. J. Low, and W. A. Goddard III, *J. Chem. Phys.*, submitted for publication.

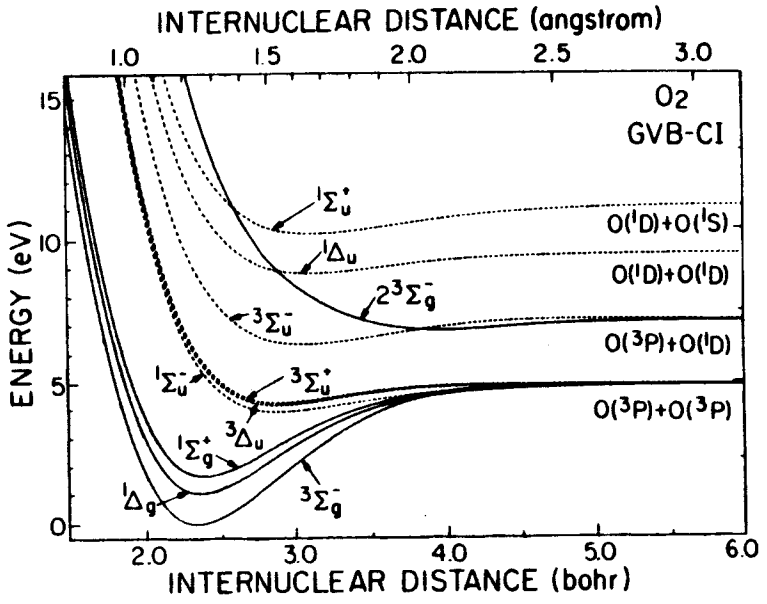

Figure 1. Bonding curves for the lower electronic states of O_2. (Based on Ref. 1.)

STEPS IN OXIDATION

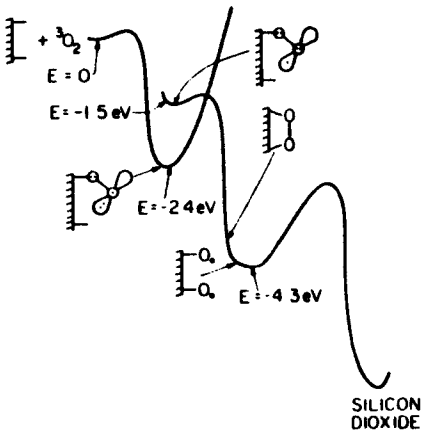

Figure 2. Initial steps in attack of O_2 on a silicon surface. (Based on Ref. 11.)

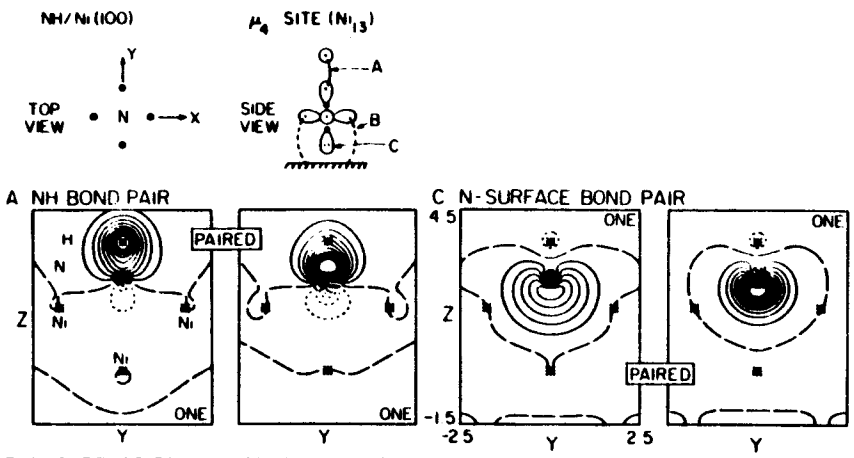

Figure 3. The GVB orbitals for NH chemisorbed at the μ_4 site (i.e., with four nearest neighbor Ni atoms) on Ni(100). (Based on calculations using an Ni_{13} cluster, Ref. 22). Solid lines indicate positive amplitude, dotted lines indicate negative amplitude, while long dashed lines indicate nodal lines. The separation between contours is 0.05 a.u.

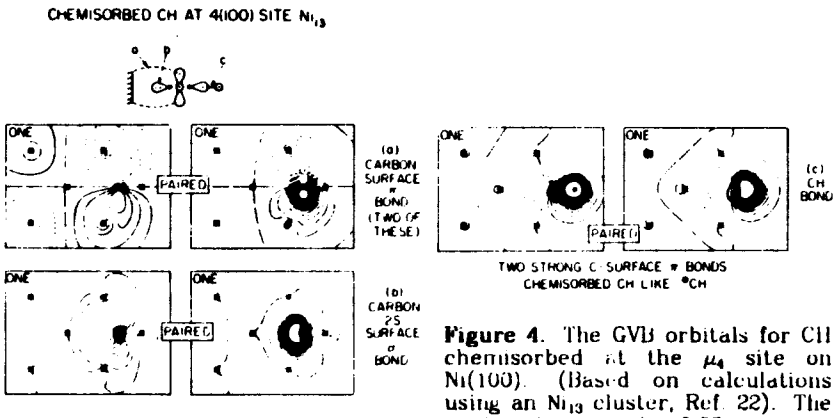

Figure 4. The GVB orbitals for CH chemisorbed at the μ_4 site on Ni(100). (Based on calculations using an Ni_{13} cluster, Ref. 22). The contour increment is 0.03 a.u.

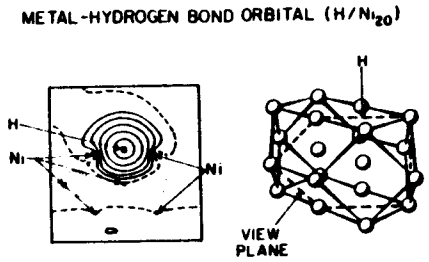

Figure 5. The GVB orbitals for H chemisorbed at the μ_4 site on Ni(100). (Based on calculations using an Ni_{20} cluster, Ref. 23b). The contour increment is 0.05 a.u.

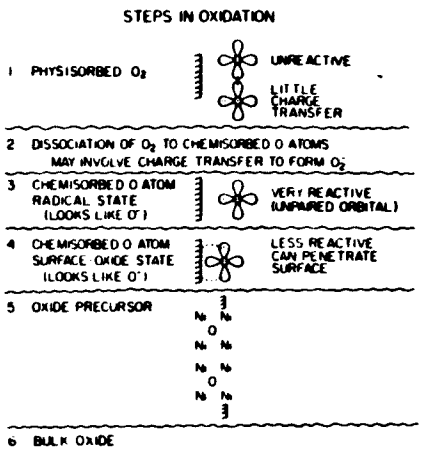

Figure 7. General steps in the oxidation of metal surfaces.

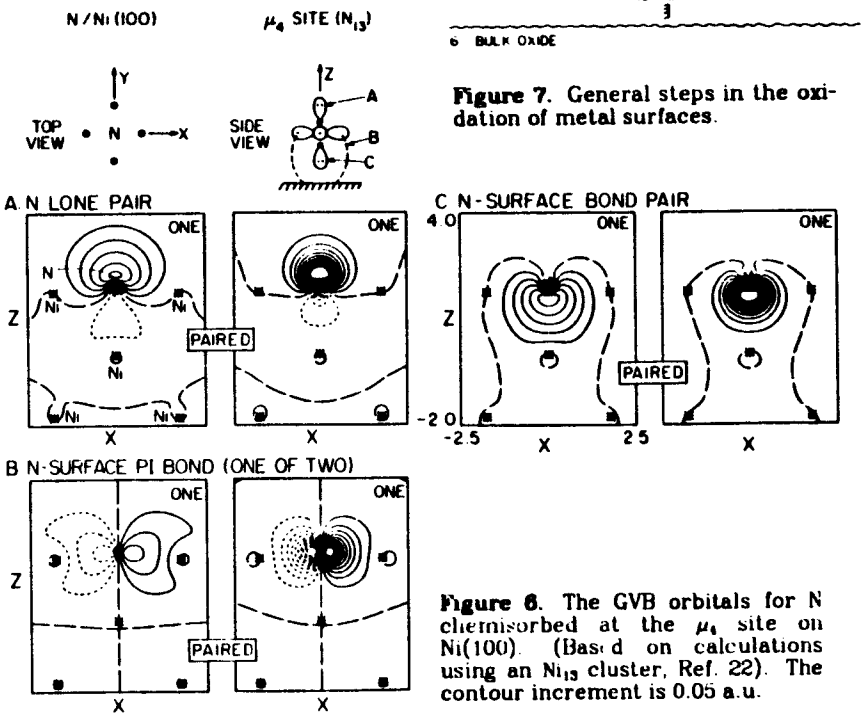

Figure 6. The GVB orbitals for N chemisorbed at the μ_4 site on Ni(100). (Based on calculations using an Ni_{13} cluster, Ref. 22). The contour increment is 0.05 a.u.

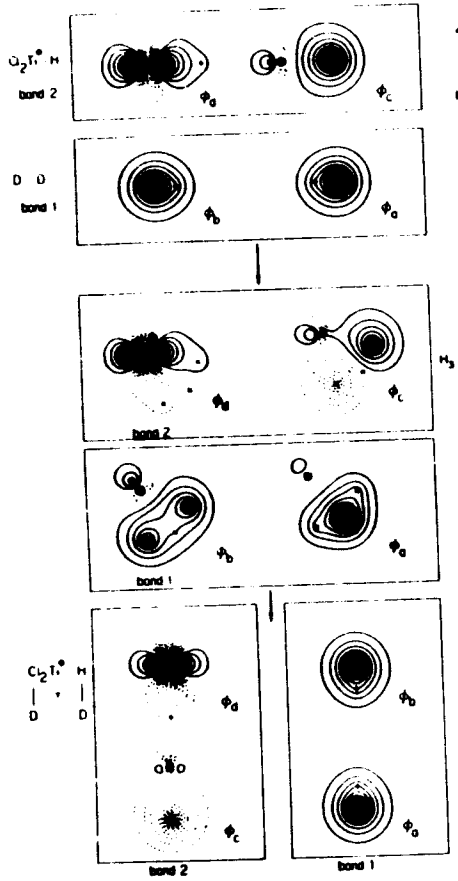

Figure 8. The orbitals for the $Cl_2Ti^+-H + D_2 \rightarrow Cl_2Ti^+-D + HD$ reaction. Contour increments are 0.05 a.u. (from Ref. 35).

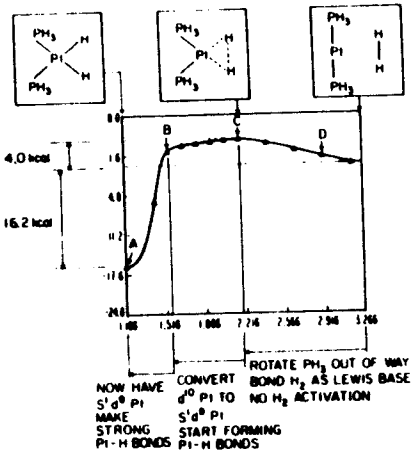

Figure 9. The potential surface for oxidative addition of H_2 to $Pt(PH_3)_2$ (from Ref. 37).

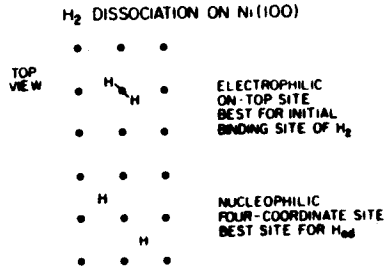

Figure 10. Site for dissociation of H_2 on Ni(100).

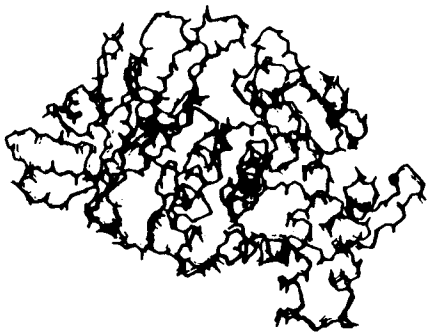

Figure 11. Comparison of theoretical (Ref. 44) and experimental (Ref. 45) structures of thermolysin.

Figure 12. Comparison of theoretical (Ref. 44) and experimental (Ref. 45) structures of thermolysin with only the C_α linkages displayed.

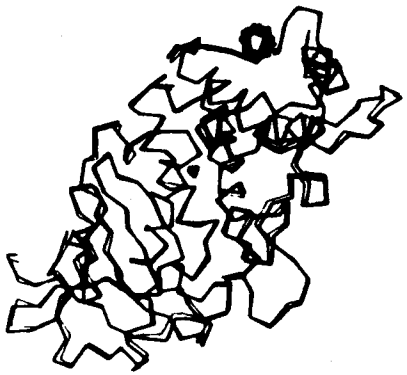

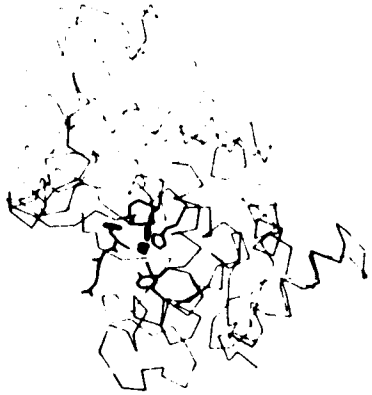

Figure 13. Structure of thermolysin with an inhibitor bound at the active site.

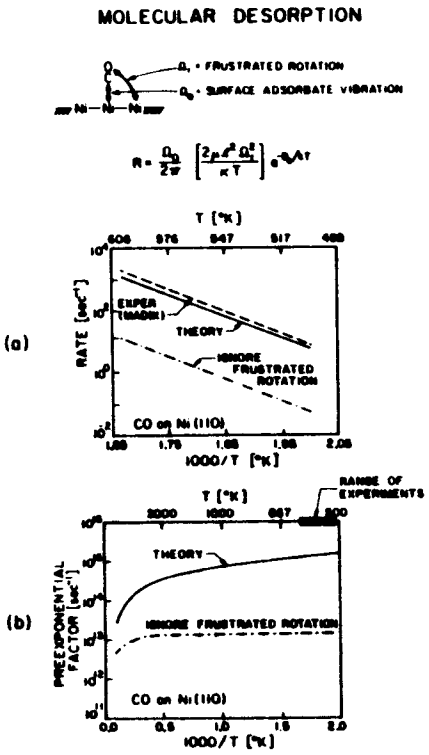

Figure 14. (a) Desorption rates for CO on Ni(110). Based on Ref. 41. The experimental results are those of C. R. Helms and R. J. Madix, *Surf. Sci.*, **52**, 577 (1975). (b) Temperature dependence of the preexponential factor for CO desorbing from Ni(110). The dashed line results from treating CO as an atom, while the solid line includes the effect of frustrated rotation.

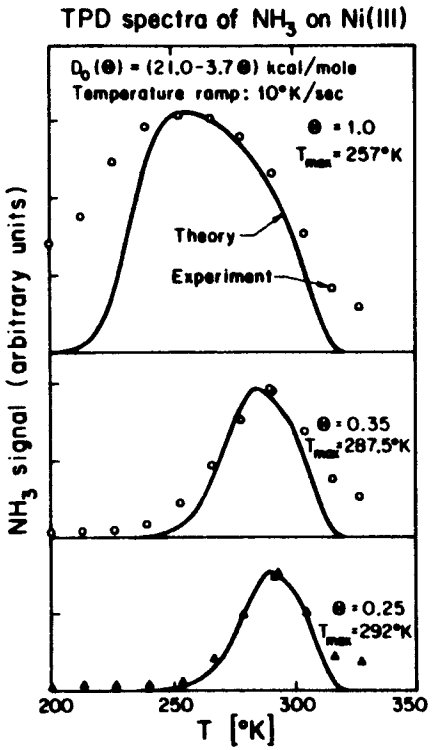

Figure 15. Comparison of theoretical (solid lines) and experimental (circles) results for temperature programmed desorption of NH_3 for Ni(111) surfaces (from Ref. 48).

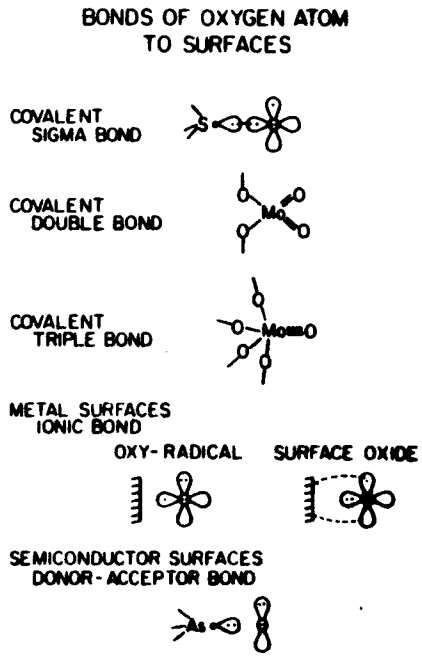

Figure 16. Bonding of oxygen atoms to surfaces.